

A Method to Calculate Fission-Fragment Yields $Y(Z, N)$ versus Proton and Neutron Number in the Brownian Shape-Motion Model

Application to calculations of U and Pu charge yields

Peter Möller¹ and Takatoshi Ichikawa^{2a}

¹ Theoretical Division, Los Alamos National Laboratory, Los Alamos, NM 87545, USA

² Yukawa Institute for Theoretical Physics, Kyoto University, Kyoto 606-8502, Japan

Received: date / Revised version: date

Abstract. We propose a method to calculate the two-dimensional (2D) fission-fragment yield $Y(Z, N)$ versus both proton and neutron number, with inclusion of odd-even staggering effects in both variables. The approach is to use Brownian shape-motion on a macroscopic-microscopic potential-energy surface which, for a particular compound system is calculated versus four shape variables: elongation (quadrupole moment Q_2), neck d , left nascent fragment spheroidal deformation ϵ_{f1} , right nascent fragment deformation ϵ_{f2} and two asymmetry variables, namely proton and neutron numbers in each of the two fragments. The extension of previous models 1) introduces a method to calculate this generalized potential-energy function and 2) allows the correlated transfer of nucleon pairs in one step, in addition to sequential transfer. In the previous version the potential energy was calculated as a function of Z and N of the compound system and its shape, including the asymmetry of the shape. We outline here how to generalize the model from the “compound-system” model to a model where the emerging fragment proton and neutron numbers also enter, over and above the compound system composition.

PACS. 25.85.Ca describing text of that key – 24.10.Lx describing text of that key – 24.75.+i describing text of that key – 25.85.Jg describing text of that key

1 Introduction

In previous investigations it has been shown that a realistic description of the experimentally observed fission-fragment charge distributions can be obtained by means of random walks on tabulated five-dimensional (5D) potential-energy surfaces calculated for a densely spaced grid for over five million different shapes [1–3]. It was particularly encouraging that the 70 charge-yield distributions measured at GSI [4] were well reproduced, including the transition from symmetric fission for light Th isotopes to asymmetric fission for the heavier isotopes beyond $A \approx 226$. However, the often strongly fluctuating patterns of odd-even staggering were not possible to obtain in that implementation of the model. Briefly stated, the reason was that there was no mechanism that allowed the properties of the two nascent fragments to affect the calculated potential-energy surface. For example, pairing was treated for the compound system as a whole.

In the literature there have been numerous discussions of odd-even staggering and models proposed to quanti-

tatively describe this feature. For example the effect has been correlated with Coulomb-related quantities, such as Z^2/A and $Z^2/A^{1/3}$, referred to as order parameters, and to pairing effects on the nuclear level density and its variation with excitation energy, see Refs. [5–7] and references therein. Other models are based on properties of separated fragments and thermal equilibrium at scission. For a review see Ref. [8]. Common for these models are that they are not based on detailed, calculated potential-energy surfaces or dynamical evolution on such surfaces. The models often also contain a substantial number of postulated terms with parameters which are determined from adjustments to observed yields. Another group of models do treat dynamical evolution, in a Langevin approach. Until now they are based on macroscopic potential-energy surfaces. or, when shell effects are included the calculations are performed for three shape variables for fairly high excitation energies ($E^* = 20$ MeV), see Ref. [9] for a brief review but with extensive references to original work.

In the Brownian shape-motion (BSM) model the only parameters are those of a well-established macroscopic-microscopic model used to calculate the five-dimensional (5D) potential-energy surfaces [10] in which the param-

Send offprint requests to:

^a Present address: Insert the address here if needed

ters have been unchanged since 2002 [11], the additional critical neck radius at which the mass split is frozen, a weak bias potential (but the results are fairly insensitive both to the magnitude of the critical neck radius and to the bias potential strength [1,2]), and two parameters in a “suppression factor” that accounts for the decrease of the shell-plus-pairing correction with energy [3].

We have recently shown that the observed magnitude of the odd-even staggering can be directly correlated to the excitation energy above the outer part of the calculated potential-energy surface [12]. Therefore we suggested the BSM model could describe odd-even staggering if a potential-energy model were developed that accounts for how the individual nascent fragment properties are expressed in the calculated potential-energy surface [12].

Here we propose a model for the potential-energy surface in which the properties of the individual fragments gradually emerge as the scission configuration is approached and specify the full details this proposed model. To treat odd-even staggering we add to the potential energy, as is customarily done since the dawn of nuclear mass calculations [13,14], a pairing contribution Δ to emerging odd fragments. However, since we start our trajectories at the ground-state shape of the even-even parent nuclei, where there is no odd pairing effect, only a fraction of the pairing delta of the fully formed final fragments is added in the initial stages of division. This fraction grows with decreasing neck diameter, see below for further discussion and specification.

We also introduce a correlated transfer of paired nucleon configurations. Such correlated nucleon transfers, which are different from sequential transfers, are often identified in nuclear reaction experiments, for a discussion see the presentation in Ref. [15] and the many references cited therein, for example Refs. [16,17].

It turns out that we can incorporate our new ideas in calculations of charge yields, with minimal modifications of existing computer codes. Our first results on charge distributions are presented below.

2 Shape parameterization and notations

To describe the nuclear shape we use the three-quadratic-surface (3QS) parameterization. It was introduced almost 50 years ago [18]. It is much more cumbersome to deal with than, say, a multipole expansion such as the β parameterization [19], but is used to allow a realistic description of shapes of a fissioning nucleus up to and including division of the single shape into separated fragments. Particularly noteworthy is that the emerging fragment shapes can be deformed spheroids or exact spheres. The latter is of special importance because it allows the extra binding associated with *spherical* doubly-magic nuclei to be accurately calculated. More details are found in Ref. [18]; the discussions of Figs. 1 and 2 there are particularly informative. How we design our potential-energy calculations in terms of this parameterization is detailed in Refs. [20, 10]; here we briefly summarize a few essential details.

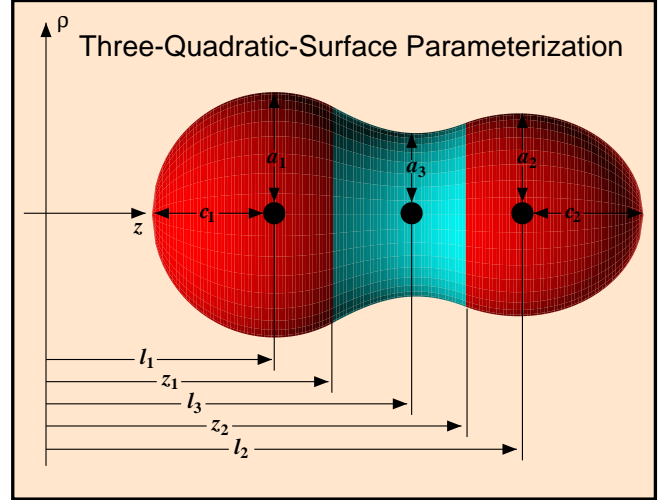


Fig. 1. Shape generated by the three-quadratic-surface parameterization. Different colors distinguish between the shape sections generated by the three expressions in Eq. (1).

In the (3QS) parameterization the shape of the nuclear surface is specified in terms of three smoothly joined portions of quadratic surfaces of revolution. They are completely specified [18] by

$$\rho(z)^2 = \begin{cases} a_1^2 - \frac{a_1^2}{c_1^2}(z - l_1)^2 & , l_1 - c_1 \leq z \leq z_1 \\ a_2^2 - \frac{a_2^2}{c_2^2}(z - l_2)^2 & , z_2 \leq z \leq l_2 + c_2 \\ a_3^2 - \frac{a_3^2}{c_3^2}(z - l_3)^2 & , z_1 \leq z \leq z_2 \end{cases} \quad (1)$$

Here the left-hand surface is denoted by the subscript 1, the right-hand one by 2 and the middle one by 3. Shapes 1 and 2 are spheroids, for which c is the semi-symmetry axis length, a is the semi-transverse axis length, and l specifies the location of the center of the spheroid. The middle body may be a spheroid or a hyperboloid of one sheet, for which c_3 is imaginary. At the left and right intersections of the middle surface with the end surfaces the value of z is z_1 and z_2 , respectively. Surfaces 1 and 2 are also referred to as end bodies and, alternatively, nascent fragments. A shape generated by the parameterization in Eq. (1) is shown in Fig. 1.

In our calculations we use five shape parameters: elongation in terms of quadrupole moment Q_2 , left and right fragment spheroidal deformations ϵ_{f1} and ϵ_{f2} , neck diameter d and mass asymmetry α_g . These five parameters completely specify the shape for which the potential energy is calculated and have been extensively discussed in Ref. [10]. Also, they completely exhausted the shape space available to this parameterization (except, trivially, for including larger values in each of the five shape parameters). For our studies here we need to revisit the asymmetry variable α_g which is directly connected to the asymmetry of nuclear shape (and the separated fragments):

$$\alpha_g = \frac{a_1^2 c_1 - a_2^2 c_2}{a_1^2 c_1 + a_2^2 c_2}. \quad (2)$$

This is equivalent to

$$\alpha_g = \frac{M_1^c - M_2^c}{M_1^c + M_2^c} \quad (3)$$

where M_1^c and M_2^c are the volumes inside the end-body quadratic surfaces, were they completed to form closed-surface spheroids and “c” in the notation is to clarify we are referring to quantities of the compound single-shape system. To avoid the introduction of a large number of equivalent concepts we use somewhat interchangeably, “mass”, “volume” and nucleon number A .

Our random-walk tracks end at a point where the neck radius of the nuclear shape is quite well developed, namely at 2.5 fm (compare to the radius of a spherical ^{240}Pu nucleus which is 7.2 fm), so the shape has almost reached the configuration of separated fragments. The neck radius is actually smaller than the radius of ^{16}O for which the radius is 2.92 fm, and which is the lightest nucleus to which we have applied the macroscopic-microscopic method. Although M_1^c and M_2^c for shapes with well-developed necks can be expected to be close to the final fragment masses we cannot directly compare M_1^c and M_2^c to the observed fission fragment masses M_1^s and M_2^s (where the superscript “s” indicates we refer to the separated fragments) because the former do not quite sum up to the total nuclear volume or mass A . However, by scaling M_1^c and M_2^c so that their sum adds up to the total mass number A , we can directly relate the “mass asymmetry” of the compound-nucleus shape to the observed heavy and light fragment masses. We obtain trivially

$$\begin{aligned} M_1^s &= r_s M_1^c = A \frac{1 + \alpha_g}{2} \\ M_2^s &= r_s M_2^c = A \frac{1 - \alpha_g}{2} \quad \text{and} \\ r_s &= \frac{A}{M_1^c + M_2^c} \end{aligned} \quad (4)$$

where r_s is a scaling factor for a nucleus with A nucleons. The scaling is equivalent to assigning the mass in the neck region to the left and right nascent fragments in proportion to the respective volumes of these nascent fragments, were they completed to closed spheroids. The amount of matter involved is in the range of 10–20 nucleons. It is obvious how the same definitions apply to the proton and neutron numbers. The symbols Z and N are used for proton and neutron numbers of the fissioning compound system. We then have:

$$Z_2^s = Z - Z_1^s \quad \text{and} \quad N_2^s = N - N_1^s \quad (5)$$

Therefore we usually use only Z_1^s and N_1^s when we explicitly refer to the number of fragment protons and neutrons, the other fragment proton and neutron numbers are then also specified. To calculate the yield as a function of both fragment proton and neutron number obviously requires that the previous 5D model (which always assumed that the proton to neutron ratios in both fragments were equal to the proton to neutron ratio in the compound system)

be generalized to 6D so that the yield $Y(Z_1^s, N_1^s, Z_2^s, N_2^s)$, which is a function of both proton and neutron asymmetry is obtained. We also realize that to describe odd-even effects requires that we space the grids we will use in terms of integer spacing of Z_1^s and N_1^s in some fashion which we will now introduce.

3 Potential energy versus shape and nascent fragment proton and neutron number

The method to calculate the two-dimensional fission-fragment yield $Y(Z, N)$ function that we now introduce is perhaps most transparently explained by occasionally referring to specific aspects of the computer code used to calculate, in the macroscopic-microscopic method, potential-energies as functions of shape. In our current potential-energy model and code we obtain a total potential energy for a specific compound nucleus (Z, N) and a specific “shape” as a sum of a macroscopic energy (given by a liquid-drop type expression) and a microscopic shell-plus-pairing correction:

$$\begin{aligned} E_{\text{pot}}(Z, N, \text{shape}) &= E_{\text{mac}}(Z, N, \text{shape}) \\ &+ E_{s+p}^{\text{prot}}(Z, (N), \text{shape}) \\ &+ E_{s+p}^{\text{neut}}((Z), N, \text{shape}) \end{aligned} \quad (6)$$

where $E_{\text{mac}}(Z, N, \text{shape})$ is the macroscopic energy and E_{s+p}^{prot} is the proton shell-plus-pairing correction and the final term the neutron shell-plus-pairing correction. In a calculation for a specific compound system and a specific shape these shell-plus-pairing corrections can trivially be individually tabulated. To obtain, say, the proton microscopic correction single-particle levels are calculated numerically in a folded-Yukawa single-particle potential with a functional form derived from the nuclear shape [21, 19]. From these levels the shell correction is obtained by use of the Strutinsky method [22, 23] and the pairing correction through, in our case, the Lipkin-Nogami method, as detailed in [24]. Thus, the proton microscopic correction is independent of neutron number, except that the potential radius and depth depend on both proton and neutron number, therefore we have used the notation (N) and (Z) to indicate a weak dependence. But for small variations of neutron number the effect on the proton *microscopic* correction is small and can be neglected, an important observation that we will make use of later. To show this insensitivity we have calculated the proton and neutron shell-plus-pairing corrections for the ground-ground state shape of $^{270}_{108}\text{Hs}_{162}$ for the single-particle fields appropriate for this nucleus. We find for the proton and neutron shell-plus-pairing corrections -3.7023 and -5.3715 MeV, respectively. When we do the calculation for single-particle fields appropriate for $^{274}_{112}\text{Cn}_{162}$ we find that the proton and neutron shell-plus-pairing corrections are -3.6305 and -5.3353 MeV respectively. So when we change the proton number by 4 units and implement the corresponding effect on the neutron single-particle field the neutron shell correction changes by only 0.0362 MeV. The change in the proton

shell-plus-pairing correction is larger because proton field changes more than the neutron field when we change the proton number.

In the fission potential-energy code the shapes that can be studied are described in terms of the three quadratic surfaces of revolution: two end spheroidal sections and a middle region that near scission is a hyperboloid of revolution [21] as discussed in the previous section, see Eq. (1) and Fig. 1. In the computer code the equations for these shapes need to be specified; five independent shape parameters are required for the shape specification. Historically the shape parameters α and σ were used [21]. But to more directly visualize the shape, we now characterize the shape in terms of five equivalent shape parameters: quadrupole moment Q_2 , related to the elongation of the shape, neck diameter d , left fragment spheroidal deformation ϵ_{f1} , right fragment spheroidal deformation ϵ_{f2} , and mass asymmetry α_g . The transformations from these parameters to the parameters of the quadratic functions that generate the shapes in the code are very lengthy and non-linear. They are described in Ref. [10]. For our discussion here we need to know that

$$\alpha_g = \frac{M_1^c - M_2^c}{M_1^c + M_2^c} = \frac{M_1^s - M_2^s}{M_1^s + M_2^s} \quad (7)$$

Rather than discussing the asymmetry in terms of nucleon number A we can use the above concepts and discuss the charge asymmetry; we have earlier assumed that the proton to neutron ratio is the same in both fragments. We now develop an approach to treat different ratios, that is if the proton and neutron numbers are Z_1^s and N_1^s in one of the fragments and $Z - Z_1^s$ and $N - N_1^s$ in the other fragment we will treat

$$\frac{Z_1^s}{N_1^s} \neq \frac{Z}{N} \neq \frac{Z - Z_1^s}{N - N_1^s} = \frac{Z_2^s}{N_2^s} \quad (8)$$

It follows from previously that when we discuss the asymmetry in terms of proton number we can write

$$\alpha_g = \frac{Z_1^s - Z_2^s}{Z_1^s + Z_2^s} \quad (9)$$

When we calculate the potential energy for the compound system that should correspond to specific (in our case integer) separated-fragment charge numbers we use Eq. (9) to define the asymmetry α_g of the corresponding compound-nucleus shape for which we calculate proton shell-plus-pairing corrections and macroscopic energies which are needed in our model. We need additional terms to describe how the macroscopic energy changes when we allow different proton to neutron ratios in the two fragments, mainly a symmetry-energy effect. We will discuss how to obtain this effect below. Correspondingly we can define the asymmetry α_g for neutrons so that it corresponds to integer splits of neutron number and tabulate the calculated neutron shell-plus-pairing corrections. Below we specify how these results serve as the starting point to obtain the potential energy for ratios between the proton and neutron numbers that are different in the two fragments.

We discussed above why the shell-plus-pairing corrections for protons and neutrons can be calculated independently of each other, to a very high degree of accuracy. Therefore we can write

$$\begin{aligned} E_{\text{pot}}(Z, N, Q_2, d, \epsilon_{f1}, \epsilon_{f2}, Z_1^s, N_1^s) = & \\ & E_{\text{mac}}(Z, N, Q_2, d, \epsilon_{f1}, \epsilon_{f2}, Z_1^s, N_1^s) \\ & + E_{s+p}^{\text{prot}}(Z, N, Q_2, d, \epsilon_{f1}, \epsilon_{f2}, \alpha_g(Z_1^s)) \quad (10) \\ & + E_{s+p}^{\text{neut}}(Z, N, Q_2, d, \epsilon_{f1}, \epsilon_{f2}, \alpha_g(N_1^s)) \\ & + E_{\text{odd}} \end{aligned}$$

Therefore, to obtain the total shell-plus-pairing corrections for any fragment split (Z_1^s, N_1^s) we calculate and tabulate the proton shell-plus-pairing corrections for a grid in α_g corresponding to integer Z_1^s (and the corresponding Z_2^s), obtained from Eq. (9). We calculate the neutron shell-plus-pairing correction for a different spacing in α_g corresponding to integer spacing in N_1^s . Thus the 6-dimensional shell-plus-pairing correction for any mass split (Z_1^s, N_1^s) is the sum of two 5-dimensional functions.

To obtain $E_{\text{mac}}(Z, N, Q_2, d, \epsilon_{f1}, \epsilon_{f2}, Z_1^s, N_1^s)$ we proceed in several steps. First, when we run the code to calculate and tabulate the proton shell-plus-pairing correction for integer values of Z_1^s we also tabulate the macroscopic energy. It will then be obtained for non-integer values

$$N_1^t = N \times \frac{Z_1^s}{Z} \quad (11)$$

of N_1^s , because the asymmetry variable α_g was chosen to correspond to integer values of Z_1^s .

Thus we have tabulated

$$E_{\text{mac}}(Z, N, Q_2, d, \epsilon_{f1}, \epsilon_{f2}, Z_1^s, N_1^t) \quad (12)$$

where we need to remember that here N_1^t corresponds to a non-integer value because the asymmetry of the shape was chosen to yield integer Z_1^s . The superscript “t” stands for “tabulated”. We need this tabulated value as one term in the macroscopic energy-model expression we now develop.

But we need to obtain the macroscopic energy for (several different) integer N_1^s . It would be difficult to obtain such macroscopic energies by developing a model that integrated across the compound nuclear shape for a configuration with variable proton and neutron densities across the shape. But we now pose that we will get a sufficiently accurate model by considering *changes* in the macroscopic energy relative to the tabulated macroscopic energy we discussed in Eq. (12). These changes are mainly due to changes in the symmetry energies, with considerably smaller contributions from other effects. We can obtain those by suitable consideration of changes in the macroscopic energy of separated fragments. These we calculate as *changes* in sum of the macroscopic energy of separated spherical fragments. Therefore we calculate the sum of the *spherical* macroscopic energies for two separated nuclei for the specific fixed Z_1^s (related to Eq. (12)) and for a number of

Table 1. Spherical fragment macroscopic energies and their sums for various fragmentations of the compound system ^{236}U leading to fragment charges 52/40; only the neutron fragmentations vary. the columns labeled E_{f1} and E_{f2} correspond the first and second term of line two in Eq. (13). The lowest sum is obtained with the proton to neutron ratio as equal as possible in the two fragments and to that of the compound system. The line corresponding to this division is indicated by a “C” in the last column.

Z_1^s	N_1^s	E_{f1}	Z_2^s	N_2^s	E_{f2}	$E_{f1} + E_{f2}$
52	96	-15.95	40	48	-84.661	-100.608
52	94	-26.35	40	50	-87.387	-113.741
52	92	-36.10	40	52	-88.671	-124.770
52	90	-45.16	40	54	-88.592	-133.751
52	88	-53.51	40	56	-87.222	-140.731
52	86	-61.12	40	58	-84.626	-145.748
52	84	-67.97	40	60	-80.868	-148.839
52	82	-74.03	40	62	-76.004	-150.032C
52	80	-79.26	40	64	-70.088	-149.348
52	78	-83.64	40	66	-63.170	-146.807
52	76	-87.12	40	68	-55.298	-142.422
52	74	-89.68	40	70	-46.515	-136.199
52	72	-91.28	40	72	-36.862	-128.143
52	70	-91.87	40	74	-26.377	-118.250
52	68	-91.42	40	76	-15.097	-106.515
52	66	-89.87	40	78	-3.055	-92.926

different N_ν :

$$E_{\text{mac}}^{\text{sep}}(Z_1^s, N_\nu, Z - Z_1^s, N - N_\nu) = E_{\text{mac}}^{\text{sph}}(Z_1^s, N_\nu) + E_{\text{mac}}^{\text{sph}}(Z - Z_1^s, N - N_\nu) \quad (13)$$

No odd-particle pairing effects should be included here; those are treated as discussed below. This function is tabulated for $Z_1^s = 52$ in Table 1 for fission of ^{236}U . We note that in this integer-spaced grid the minimum energy occurs for a split where the sum of Z/N ratios in the two fragments is as close as possible to $2 \times Z/N$ of the compound nucleus. The line corresponding to this split is indicated by a “C” at the very right.

We pose that the macroscopic energy for any fragment division (Z_1^s, N_1^s) in the fissioning system is given as

$$E_{\text{mac}}(Z, N, Q_2, d, \epsilon_{f1}, \epsilon_{f2}, Z_1^s, N_1^s) = E_{\text{mac}}(Z, N, Q_2, d, \epsilon_{f1}, \epsilon_{f2}, Z_1^s, N_1^t) + E_{\text{mac}}^{\text{sep}}(Z_1^s, N_\nu, Z - Z_1^s, N - N_\nu) - E_{\text{mac}}^{\text{sep}}(Z_1^s, N_1^t, Z - Z_1^s, N - N_1^t) \quad (14)$$

where the last term is calculated by interpolation in the table corresponding to Eq. (13). As a specific example we discuss a fragment division where the charge split is 52/40. Then $N_1^t = 81.39$. We tabulate the sum in Eq. (13) as the right column in Table 1 and plot this sum for the specific charge division in our example in Fig. 2.

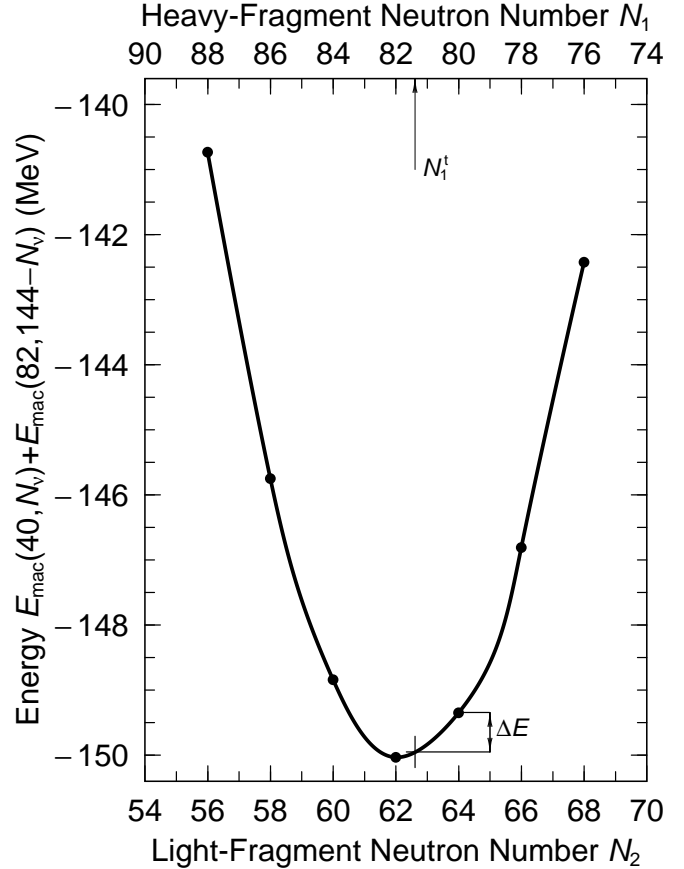


Fig. 2. Sum of separated-fragment macroscopic energies.

As an example that we can now, in our model, calculate the macroscopic energy for any (Z_1^s, N_1^s) . To illustrate this we continue to discuss our specific example. Equation 14 is a complete specification of the method. Suppose we want to calculate the macroscopic energy for the particular case $E_{\text{mac}}(92, 144, Q_2, d, \epsilon_{f1}, \epsilon_{f2}, 52, 64)$. Then we obtain the first term in the right member of Eq. (14) from our tabulated function in Eq. (12). For our choice of $N_1^s = 64$ the second term is given by the energy at the upper horizontal line and the third term by the energy at the lower horizontal line in Fig. 2. Thus in this example we obtain the macroscopic energy as a sum of the tabulated macroscopic energy plus ΔE indicated in Fig. 2.

One may argue that since some of the fissioning shapes involve deformed nascent fragments the terms in Eq. (13) should be evaluated for the corresponding deformed shapes. But for the *differences* we consider here it only makes a minuscule difference. Let us choose ^{102}Zr and ^{106}Zr in Table 1 as an illustrative example. The energy difference for the spherical shapes ΔE_{sph} tabulated is

$$\Delta E_{\text{sph}} = -63.108 - (-75.973) = 12.865 \quad (15)$$

We have evaluated the macroscopic energies for deformed shapes with $\epsilon_2 = 0.5$, which is the largest deformation for emerging fragments in our specified deformation grid, see Ref. [10] and obtain

$$\Delta E_{\text{def}} = -53.262 - (-66.108) = 12.846 \quad (16)$$

Thus, although the absolute energies change considerably the effect on their differences is completely negligible, only 0.019 MeV.

Finally we need to account for odd pairing effects in the emerging fragments. When the fragments are fully developed with zero neck radius of the compound system a common assumption is that for odd-odd splits the extra odd contribution to the energy should be $E_{\text{odd}} = 2 \times \Delta$ where Δ is the pairing-gap parameter, chosen as $\Delta = 1.0$ MeV. With a non-zero neck radius the effect of pairing of the emerging odd splits would be smaller; for very compact shapes with no obvious neck there should be no effect. This leads to the following prescription for the odd energy of the fissioning system

$$\begin{aligned} E_{\text{odd}} &= 2 \times \Delta \times (B_W - 1)^k && \text{odd } Z_1^s, Z_2^s \\ E_{\text{odd}} &= 0 && \text{even } Z_1^s, Z_2^s \end{aligned} \quad (17)$$

where, with the choice $k = 1$, $(B_W - 1)^k$ is the shape dependence of the Wigner term in our potential-energy model. The shape factor B_W is 1 for a shapes with no neck and increases continuously, as the neck develops, to 2 for separated fragments. It is necessary to postulate such a shape dependence because the macroscopic energy of two separated fragments contains two Wigner terms, the original system only one. Without such a shape dependence a discontinuity of the order of 10 MeV would occur at scission of actinide nuclei. That is, if we calculated the energy for a deforming nucleus up to the scission point we would at scission obtain a 10 MeV lower energy than if we calculated the energy of two approaching separated fragments. A pedagogical figure illustrating this and the necessity of this shape dependence is in Ref. [11], Fig. 1. Since we need a realistic potential-energy surface in the scission region we do need to consider these issues (which have in many investigations been ignored). The comprehensive discussion of the shape-dependence of the Wigner term in Ref. [25] carries directly over to how the effect of the pairing Δ increases as the neck becomes more narrow. There is no known derivation of the Wigner shape dependence so it is just postulated, but with consideration of its limiting behavior [25]. The power constant k , which we introduced here to allow some sensitivity studies, governs how early in the division process the character of the two fragments causes the “second” Wigner term, or in our case, the odd pairing effect, to manifest itself. Below we will present sensitivity studies on the shape dependence and on the magnitude of the pairing delta.

4 Application to Charge Asymmetries

A calculation of the complete (2D) $Y(Z, N)$ yield distribution based on the above model would lead to much more complex calculations compared to our current 5D implementation [1–3], because of its 6D nature and associated vastly increased storage requirements. But, as a test of the above approach, we can study many of its aspects by looking at the odd-even staggering in charge distri-

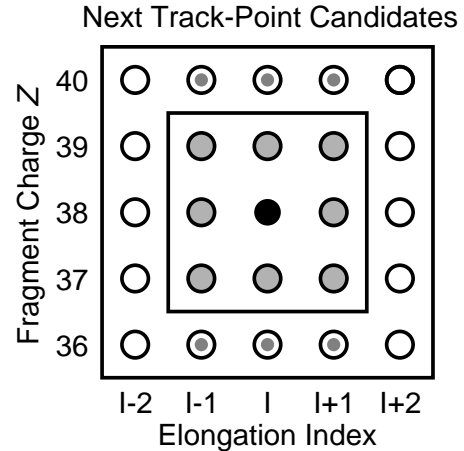


Fig. 3. Two-dimensional slice in the 5D space schematically illustrating possible candidate points for the next trajectory step. The smaller square with gray-filled circles inside, indicates the limit originally chosen for next step candidate points. The circles partially filled with gray correspond to transfer of paired configurations.

butions without treating the neutrons separately. We obviously then have to calculate the potential energy for field asymmetries α_g that correspond to integer spacing of the proton number Z_1^s . For ^{240}Pu , for each combination of the other 4 shape variables [10], we calculate the potential energies for asymmetries corresponding to charge splits 47/47, 46/48, 45/49 . . . , and accordingly for other elements. This corresponds to “averaging” or “summing” over the neutron variable, a procedure we assume has limited effects on the charge distributions obtained relative to summing over N a calculated complete 2D $Y(Z, N)$ distribution. Thus, we obtain in strict analogy with our previous results, on a discreet grid the 5D potential-energy matrix $E_{\text{pot}}(I_1, I_2, I_3, I_4, I_5)$ where I_1 corresponds to the quadrupole moment (or elongation), I_2 to the neck radius, I_3 to spheroidal deformations of one of the emerging fragments, I_4 to spheroidal deformations of the other emerging fragment, I_5 to charge asymmetries Z_1^s/Z_2^s , where the charge numbers are integers. However, since the calculated energy, E_{comp} , does not contain contributions from pairing effects in the emerging fragments we add the shape-dependent odd enhancement according to Eq. (17). It turns out very few modifications of the random walk code are required for this calculation.

In the BSM model we find the yield distributions by generating paths through the potential-energy matrix as follows. We usually start the path at the ground state (black dot in the schematic 2D Fig. 3). We then select randomly one of the 242 surrounding points (circles with gray interior in Fig. 3, only 8 of them in this schematic representation) as a candidate for the next point on the track. Suppose the energy difference between this point and the current point is ΔV . Then, if $\Delta V < 0$ the candidate point becomes the next point (and current point “at the next throw of the dice”) on the path. However, if $\Delta V > 0$ this outcome is only selected with probability $P = \exp(-\Delta V/T)$ where T is the temperature; full

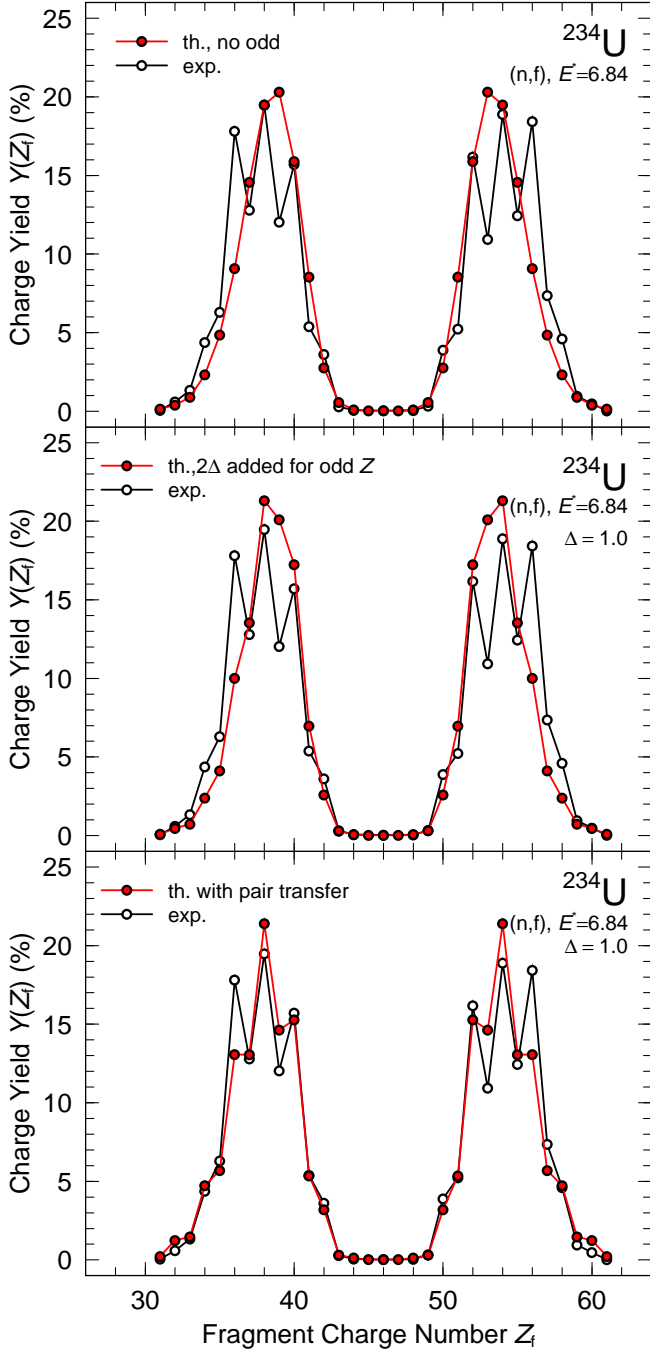


Fig. 4. Calculated and measured charge yields for neutron-induced fission of ^{234}U . The top panel represents the original model, the middle panel has $2 \times \Delta$ added to the potential energy in the matrix locations corresponding to odd charge splits. In the bottom panel steps corresponding to two-proton changes in asymmetry are allowed.

details are in Refs. [1,2]. When the critical neck radius $c_0 = 2.5$ fm is reached the walk is terminated and the asymmetry of the shape recorded. Each yield curve is based on 20000 tracks. We present results for four reactions: thermal neutron-induced fission of ^{234}U , ^{236}U , ^{240}Pu , and photon-induced fission with energies centered around 11 MeV for ^{234}U in Figs. 4, 5, 7, and 6 respec-

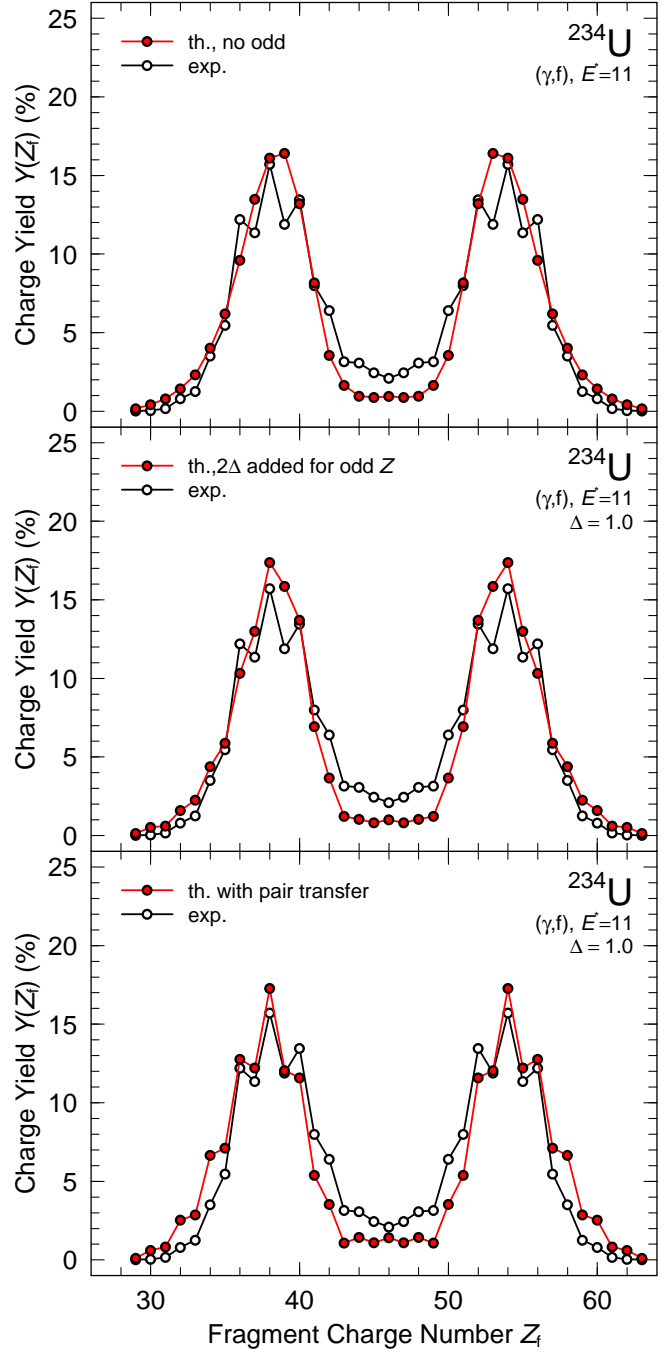


Fig. 5. As Fig. 4, but the experimental data are for (γ, f) reactions leading to $E^* \approx 8 - 14$ MeV; they include contamination from fission after $1n$ ($\approx 15\%$) and $2n$ ($\approx 5\%$) emission[4]. The calculations are for fission of ^{234}U at $E^* = 11$ MeV.

tively. The experimental data for the (n, f) reactions are from Ref. [26], the (γ, f) data from Ref. [4]. The top frame in each of the four figures is with the original model with no pairing effect added. The middle frames are based on BSM in the 5D potential modified according to Eq. (17). We find little staggering in the calculated curves, although we implemented the “standard” explanation for odd-even staggering: for odd-odd splits the potential is on average $2 \times \Delta$ (for zero neck radius; less in earlier stages of the

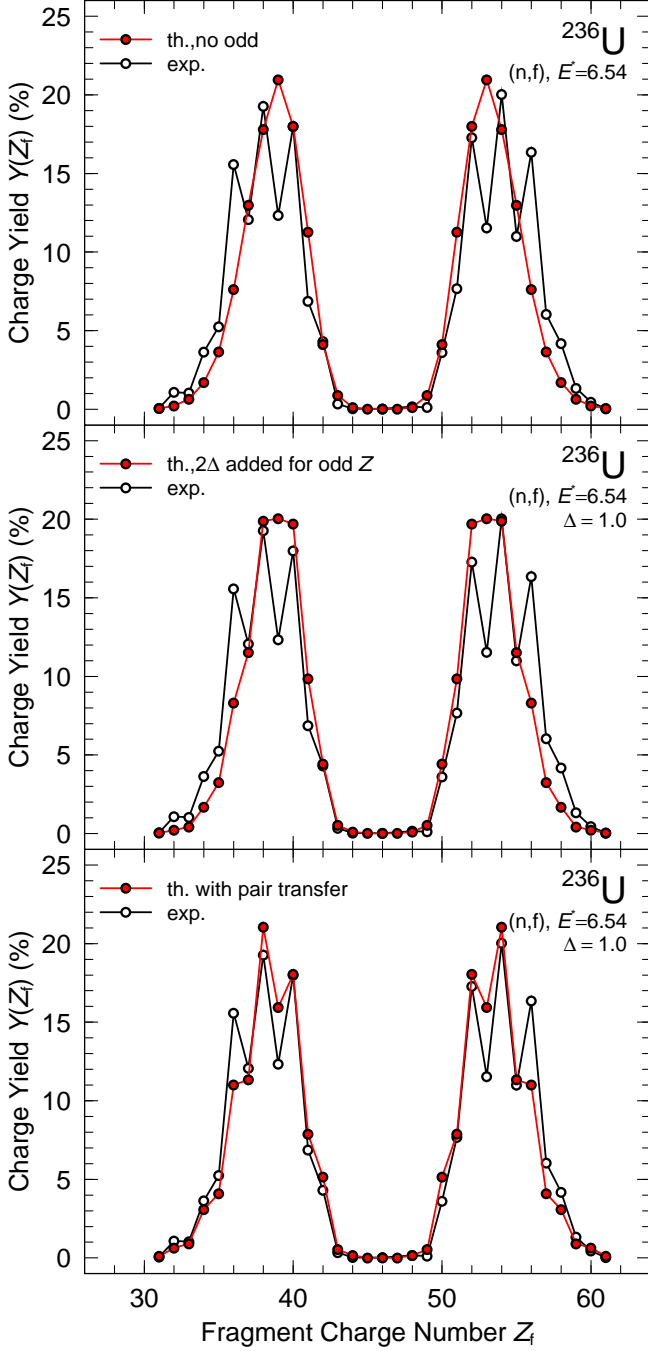


Fig. 6. As Fig. 4 but for ^{236}U .

fission process) higher than the potential for even splits. But it is clear that the original formulation of the BSM model would never be able to describe odd-even staggering, even after the addition of a pairing effect to the calculated potential energy. To illustrate why let us look at Fig. 1 and specifically at $Z = 38$ on the experimental curve. Let us assume that $Z = 38$ is the asymmetry of the current point on our evolving track. Because we only consider next-neighbor gridpoints as candidate points for the next point on the path, we have to populate $Z = 39$ which has a very low yield, to subsequently populate the high-yield $Z = 40$ point, for example. To obtain a pro-

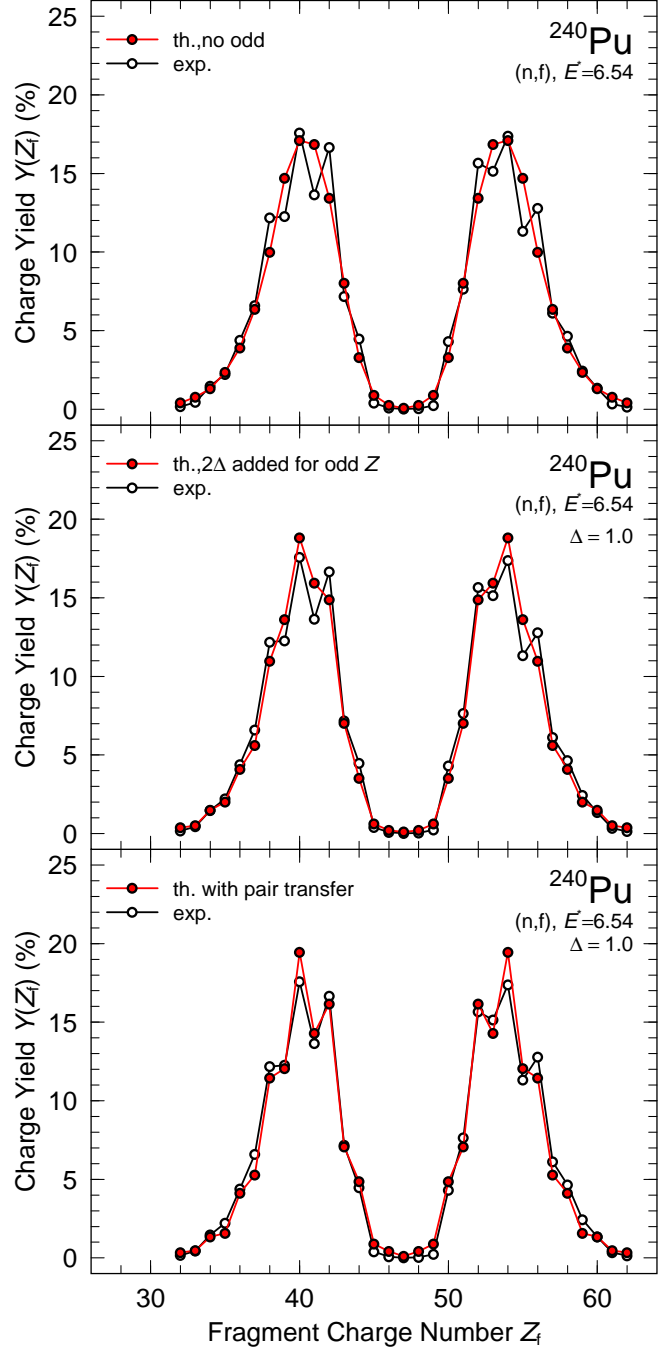


Fig. 7. As Fig. 4 but for ^{240}Pu .

nounced staggering with these model features is impossible. But as the shape evolves in the asymmetry direction and two levels cross it is reasonable that an alternative to breaking a pair and transferring only one proton between the evolving fragments is that a paired two-proton configuration could be transferred in one step. We have implemented this possibility in the BSM model by also allowing $Z - 2$ and $Z + 2$ as next track-point candidates (shown as circles partially filled with gray in Fig. 3). As alluded to above transfer reactions indicate that correlated transfer of nucleon pairs are common see Refs. [15–17]. In our current treatment transfer of either a paired config-

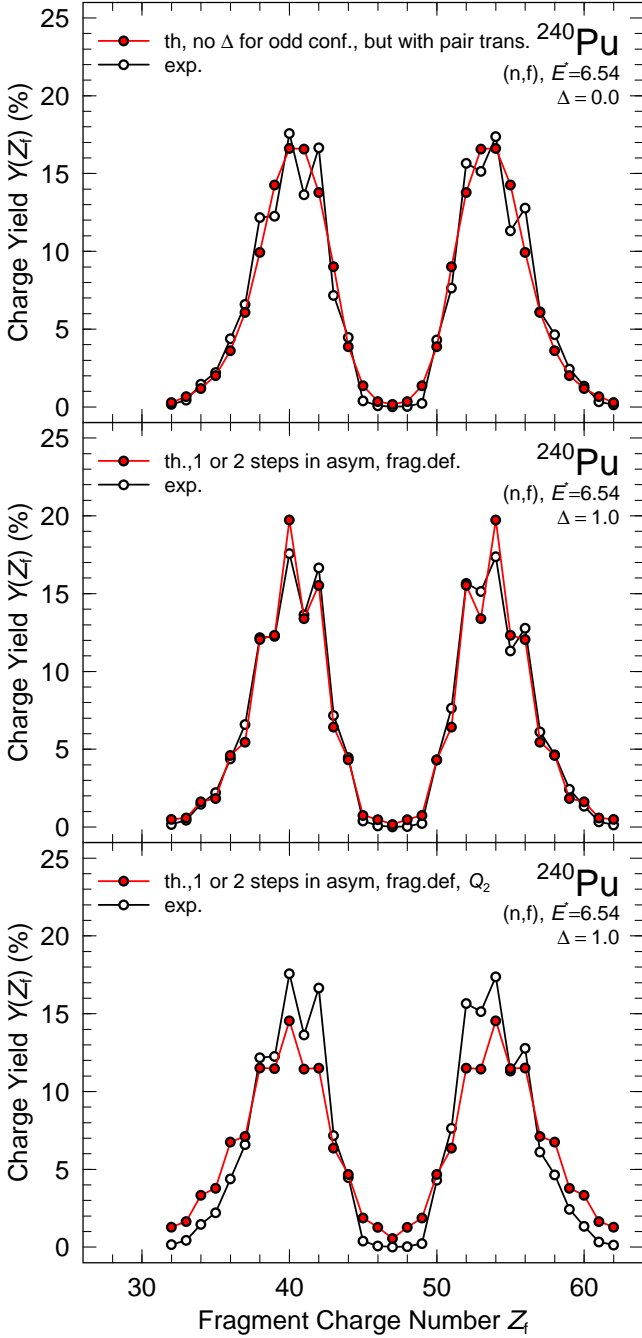


Fig. 8. Calculated charge yield for neutron-induced fission of ^{240}Pu in the BSM model for different assumptions about pairing and next-step grid-point candidates. In the top panel no pairing effect is added to the potential energy for odd splits, but one or two steps in asymmetry is implemented. In the middle panel we add a pairing effect to odd splits and permit as next step candidates one or two grid points in asymmetry and both of the fragment deformations. In the bottom panel we have also allowed one or two steps in the elongation coordinate Q_2 .

uration or breaking of a pair and transfer of one proton can occur. Typical excitation energies at the end of the asymmetric tracks, see Ref. [12] are 7.7–11.6 MeV, and

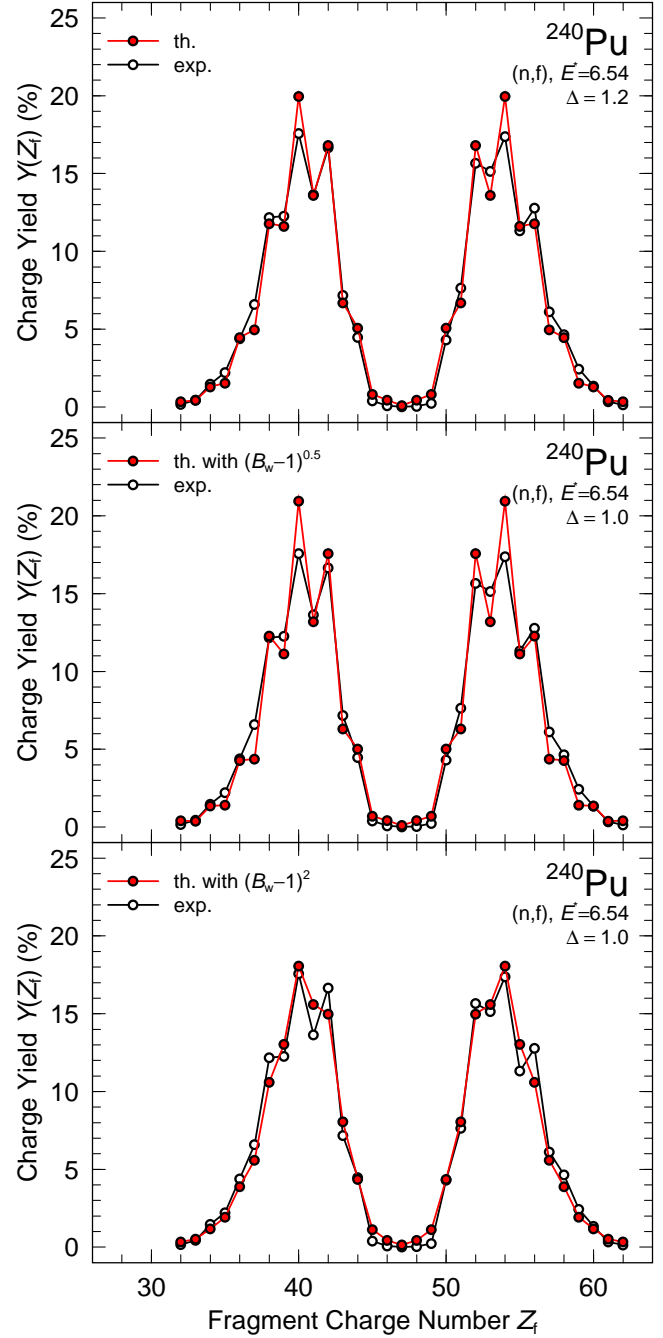


Fig. 9. Study of yield sensitivity to the magnitude of the pairing Δ and the onset of fragment pairing effects. Except for the very small pairing effects on which the bottom panel is based the results are quite robust and similar to the standard result in the bottom panel in Fig. 7.

lower earlier in the shape evolution. Our consideration of paired configurations is quite consistent with the results of Ref. [27], where in one example at 8.4 MeV excitation the proportion of paired configurations is 36%.

The calculated yields with transfers of correlated pairs allowed as next track-point candidates are in the bottom panels in Figs. 4–7. Staggering is now obvious in the calculated results and in close agreement with the experi-

mental data. In the calculated results in Figs. 4–7 it may seem that the crucial generalization that we introduced to describe the odd-even staggering is not the first step we took, namely the addition of $2 \times \Delta$ to the odd charge splits, but the second step in which we permitted a change in Z of two units, corresponding to a transfer of a paired proton configuration. But what if we had implemented this as a first step? We have investigated this possibility and show in the top panel of Fig. 8 the calculated charge yield for neutron-induced fission of ^{240}Pu with no pairing energy added to the odd charge splits, but with both one and two steps in Z permitted as next candidate points on the random-walk trajectory. There is no odd-even staggering in the calculated curve which is extremely similar to the calculated yield in the top panel in Fig. 7. It is interesting to observe that although allowing both one and two steps in Z effectively corresponds to increasing the speed of motion in asymmetry, or equivalently increasing the distance between grid points, there is little change in the calculated yield curve. In the middle panel of Fig. 8 we have added (fractions of) 2Δ to the potential energies for odd charge splits, allow one or two steps in asymmetry, but also allow one or two steps in the fragment deformation shape variables. There is little difference compared to the bottom panel in Fig. 7. This again shows, as was earlier pointed out [2] that the calculated yield curves in the BSM model do not depend sensitively on most changes in the deformation grid. In the bottom panel of Fig. 8 we have furthermore allowed one or two steps in the elongation variable Q_2 . In this case there is a noticeable effect on the calculated yield. Now the calculated distribution is slightly wider than the experimental results. In Ref. [2] we showed that tripling the number of points in Q_2 led to a calculated distribution that was narrower than the experimentally observed one. Obviously, extreme changes in the grid will influence the calculated results. For example if we were to use only three grid points in the elongation variable we would not obtain realistic yields.

Finally we study, for ^{240}Pu , the sensitivity to variations of the postulated shape dependence that governs the onset of odd-even effects on the potential energy and to the magnitude of the pairing Δ . The results are shown in Fig. 9. The top panel shows the effect of increasing the pairing Δ by 20% relative to our standard assumption of $\Delta = 1.0$ MeV. The calculated curve is little different for the result in the bottom panel of Fig. 7. Therefore the exact choice of Δ is a non-issue in this first study of odd-even staggering. In larger systematic studies a well-defined prescription should obviously be introduced. The middle and bottom panels show the results for different forms of the shape factor $(B_W - 1)^k$ which governs the rate with which the effect of the odd-even pairing Δ in the fragments affects the calculated potential energy as scission is approached. The quantity B_W is close to 1.5 at our selected scission configuration. Therefore, in the middle panel the factor $(B_W - 1)^{0.5}$ is 0.7, so that for the odd configurations 1.4 MeV is added, less earlier in the division process. The staggering here is only very slightly larger than in our standard calculation in the bottom panel of Fig. 7 where 1.0 MeV is

added in the scission region. In the bottom panel of Fig. 9 the shape factor $(B_W - 1)^2$ comes out to 0.25 so that only 0.5 MeV or less is added to the odd-odd divisions. Here the staggering is much reduced, as might be expected. However from these sensitivity studies we conclude that the results are quite robust for reasonable variations of the assumptions about the onset of fragment character on the potential energy as well as to the magnitude of the pairing Δ .

In summary we have shown that to describe odd-even staggering in the BSM model we must add simultaneously two effects: (1) odd-even effects on the calculated potential-energy surface and (2) allow transfers of correlated paired proton configurations; they work together in the development of odd-even staggering.

As future “perspectives for the next decade” we anticipate that to develop more accurate descriptions we need to

- implement the extensions we discuss here into a computer model framework and calculate the full $Y(Z, N)$ fission-fragment yield distributions (a two-dimensional function of neutron and proton number),
- treat from more basic principles how the number of paired configurations decrease with excitation energy (see Ref. [27] for a discussion) which should influence the probability with which a point corresponding to two-nucleon transfer is chosen as the next candidate point on the trajectory,
- calculate the damping of shell effects based on actual single-particle structure rather than use a parameterized approach.
- understand issues related to the deformation grid. Clearly the calculated yields do depend on the selection of the grid. To take an obvious example, were we to have only 3 grid points in the elongation direction we would not obtain any realistic yields. However, in the extensive sensitivity studies in Ref. [2] it was shown that the yields were remarkably insensitive to many types of grid changes, as is also shown by the results of Figs. 8 and 9 above.

Discussions with A. Sierk, A. Iwamoto, and J. Randrup are appreciated. This work was supported by travel grants for P.M. to JUSTIPEN (Japan-U.S. Theory Institute for Physics with Exotic Nuclei) under grant number DE-FG02-06ER41407 (U. Tennessee). This work was carried out under the auspices of the NNSA of the U.S. Department of Energy at Los Alamos National Laboratory under Contract No. DE-AC52-06NA25396. TI was supported in part by MEXT SPIRE and JICFuS and JSPS KAKENHI Grant no. 25287065.

References

1. J. Randrup and P. Möller, Phys. Rev. Lett. **106** (2011) 132503.
2. J. Randrup, P. Möller, and A. J. Sierk, Phys. Rev. C **84** (2011) 034613.
3. J. Randrup and P. Möller, Phys. Rev. C **88** (2013) 064606.

4. K.-H. Schmidt, S. Steinhäuser, C. Böckstiegel, A. Grewe, A. Heinz, A. R. Junghans, J. Benlliure, H.-G. Clerc, M. de Jong, J. Müller, M. Pfützner, and B. Voss, Nucl. Phys. **A665** (2000) 221.
5. J. P. Bocquet and R. Brissot, Nucl. Phys. **A502** (1989) 213c.
6. F. Rejmund, A.V. Ignatyuk, A.R. Junghans, K.-H. Schmidt Nucl. Phys. A **678** (2000) 215.
7. M. Caamaño, F. Rejmund, and K.-H. Schmidt, J. Phys. G: Nucl. Part. Phys. **38** (2011) 035101.
8. J. Benlliure, A. Grewe, M. de Jong, K.-H. Schmidt, and S. Zhdanov, Nucl. Phys. A **628** (1998) 458.
9. P. Möller, J. Randrup, Phys. Rev. C **91** (2015) 044316.
10. P. Möller, A. J. Sierk, T. Ichikawa, A. Iwamoto, R. Bengtsson, H. Uhrenholt, and S. Åberg, Phys. Rev. C **79** (2009) 064304.
11. P. Möller, A. J. Sierk, and A. Iwamoto, Phys. Rev. Lett. **92** (2004) 072501.
12. P. Möller, J. Randrup, A. Iwamoto, and T. Ichikawa, Phys. Rev. C **90** (2014) 014601.
13. C. F. von Weizsäcker, Z. Phys. **96** (1935) 431.
14. H. A. Bethe and R. F. Bacher, Rev. Mod. Phys. **8** (1936) 82.
15. <https://indico.cern.ch/event/183702/contribution/2/material/slides/0.pdf>.
16. W. von Oertzen and A. Vitturi, Rep. Prog. Phys. **64** (2001) 1247.
17. L. Corradi, S. Szilner, G. Pollarolo, G. Colò, P. Mason, E. Farnea, E. Fioreto, A. Gadea, F. Haas, D. Jelavić-Malenica, N. Mărginean, C. Michelagnoli, G. Montagnoli, D. Montanari, F. Scarlassara, N. Soić, A. M. Stefanini, C. A. Ur, and J. J. Valiente-Dobón, Phys. Rev. C **84** (2011) 034306.
18. J. R. Nix, Nucl. Phys. **A130** (1969) 241.
19. P. Möller, J. R. Nix, W. D. Myers, and W. J. Swiatecki, Atomic Data Nucl. Data Tables **59** (1995) 185.
20. P. Möller, D. G. Madland, A. J. Sierk, and A. Iwamoto, Nature **409** (2001) 785.
21. M. Bolsterli, E. O. Fiset, J. R. Nix, and J. L. Norton, Phys. Rev. C **5** (1972) 1050.
22. V. M. Strutinsky, Nucl. Phys. **A95** (1967) 420.
23. V. M. Strutinsky, Nucl. Phys. **A122** (1968) 1.
24. P. Möller and J. R. Nix, Nucl. Phys. **A536** (1992) 20.
25. P. Möller, J. R. Nix, and W. J. Swiatecki, Nucl. Phys. **A492** (1989) 349.
26. M.B. Chadwick, P. Oblozinsky, M. Herman, N.M. Greene, R.D. McKnight, D.L. Smith, P.G. Young, R.E. MacFarlane, G.M. Hale, R.C. Haight, S. Frankle, A.C. Kahler, T. Kawano, R.C. Little, D.G. Madland, P. Möller, R. Mosteller, P. Page, P. Talou, H. Trellue, M. White, W.B. Wilson, R. Arcilla, C.L. Dunford, S.F. Mughabghab, B. Pritychenko, D. Rochman, A.A. Sonzogni, C. Lubitz, T.H. Trumbull, J. Weinman, D. Brown, D.E. Cullen, D. Heinrichs, D. McNabb, H. Derrien, M. Dunn, N.M. Larson, L.C. Leal, A.D. Carlson, R.C. Block, B. Briggs, E. Cheng, H. Huria, K. Kozier, A. Courcelle, V. Pronyaev, S.C. van der Marck (CSEWG Collaboration), Nuclear Data Sheets, **107** (2006) 2931.
27. H. Uhrenholt, S. Åberg, A. Dobrowolski, Th. Døssing, T. Ichikawa, and P. Möller, Nucl. Phys. A **913** (2013) 127.